Hindawi Publishing Corporation
Journal of Petroleum Engineering
Volume 2016, Article ID 1708929, 14 pages
http://dx.doi.org/10.1155/2016/1708929

Research Article

Effect of Pore-Scale Heterogeneity and Capillary-Viscous Fingering on Commingled Waterflood Oil Recovery in Stratified Porous Media

Emad W. Al-Shalabi and B. Ghosh

Petroleum Engineering Department, The Petroleum Institute, Abu Dhabi, UAE

Correspondence should be addressed to Emad W. Al-Shalabi; emalshalabi@pi.ac.ae

Received 23 February 2016; Accepted 4 May 2016

Academic Editor: Chih-Ming Kao

Oil recovery prediction and field pilot implements require basic understanding and estimation of displacement efficiency. Corefloods and glass micromodels are two of the commonly used experimental methods to achieve this. In this paper, waterflood recovery is investigated using layered etched glass micromodel and Berea sandstone core plugs with large permeability contrasts. This study focuses mainly on the effect of permeability (heterogeneity) in stratified porous media with no cross-flow. Three experimental setups were designed to represent uniformly stratified oil reservoir with vertical discontinuity in permeability. Waterflood recovery to residual oil saturation (S_{or}) is measured through glass micromodel (to aid visual observation), linear coreflood, and forced drainage-imbibition processes by ultracentrifuge. Six oil samples of low-to-medium viscosity and porous media of widely different permeability (darcy and millidarcy ranges) were chosen for the study. The results showed that waterflood displacement efficiencies are consistent in both permeability ranges, namely, glass micromodel and Berea sandstone core plugs. Interestingly, the experimental results show that the low permeability zones resulted in higher ultimate oil recovery compared to high permeability zones. At S_{or} microheterogeneity and fingering are attributed for this phenomenon. In light of the findings, conformance control is discussed for better sweep efficiency. This paper may be of help to field operators to gain more insight into microheterogeneity and fingering phenomena and their impact on waterflood recovery estimation.

1. Introduction

Waterflooding is still the most economically advantageous, secondary oil recovery method. The efficiency and sustainability of a waterflood project is numerically assessed by the recovery efficiency, represented as the product of the displacement sweep efficiency by volumetric sweep efficiency of flooding water. It is defined as [1]

$$\mathrm{RE} = E_{\mathrm{D}} E_{\mathrm{V}} = E_{\mathrm{D}} E_{\mathrm{A}} E_{\mathrm{I}}, \tag{1}$$

where RE is the recovery efficiency; E_{D} is the displacement sweep efficiency, which is the fraction of oil displaced from a contacted volume of reservoir. E_{V} is the volumetric sweep efficiency, which represents the fraction of the reservoir pore volume contacted by the injected water at a given time. E_{V} is the product of the areal sweep efficiency (E_{A}) with the vertical sweep efficiency (E_{I}). E_{A} is the fraction of the area of flood pattern swept by water. It depends on flooding pattern, water-oil mobility ratio, and volume of water injected. E_{I} is the fraction of vertical cross-sectional area of the reservoir between injector and producer wells which is swept by water at a given time. The vertical sweep efficiency depends heavily on heterogeneity of the reservoir rock [2].

Because of the variation of depositional environment, sedimentary rocks are often found in layers with random variation in their flow characteristics. These layers or strata may have vertical communication (Figure 1(a)) or may be vertically sealed with extremely low permeable rock (Figure 1(b)). Reservoir heterogeneity might negatively affect waterflood recovery efficiency through two different ways:

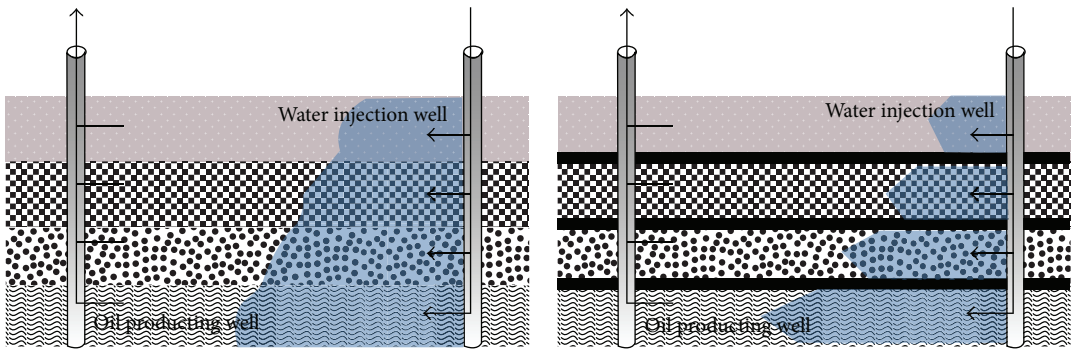

(a) With vertical communication (no flow barrier)

(b) Without vertical communication (barriers between layers)

Figure 1: Injection-production vertical well pair in a stratified reservoir.

(1) channeling and fingering of water through the oil bank which leads to bypassing oil zones (areal sweep issue) and (2) disproportionate flow of flood water through different strata, resulting in early water breakthrough in the high permeability stratum, while the low permeability stratum remains largely unswept (vertical sweep issue).

Channeling is even more pronounced when the interface between displacing and displaced fluids is unstable because of the adverse mobility ratio, which causes viscous fingering [3]. Adverse mobility ratio occurs when the mobility of the displacing fluid (water) is higher than the mobility of the displaced fluid (oil). Other factors that control this phenomenon include displacement velocity, geometry and dimensions of the porous media, capillary and gravitational forces, rock permeability, and wettability [4]. The disproportionate flow of flood water through different strata occurs when there is a large permeability contrast between the strata. To reduce this disproportionate flow of waterflood, different profile modification techniques such as polymer gels and microgels are applied [5–8].

A layered or stratified reservoir may consist of several beds or sheets, some of which may be field-wide, while others are pinch-outs. In a stratified reservoir, the waterflood performance and recovery efficiency may be poor and difficult to predict if there is a large permeability contrast between the layers [9]. In most cases, stratified reservoirs possess vertical continuity; however, there are many with barriers to vertical flow. To the best of our knowledge, most waterflood performance is studied in stratified communicating reservoirs [2, 10] with very few reported studies on stratified reservoirs with vertical discontinuity. It is worth mentioning that the enormous works done on waterflood performance on heterogeneous reservoir with vertical discontinuity based on Dykstra-Parson and Styles method are based on the assumption of piston like displacement, ignoring the aspect of microscopic displacement efficiency, which is the focus of this study.

In this study, the effect of permeability contrast on commingled waterflood performance in a stratified porous medium is investigated through three different experimental methods. The methods include visual observations through glass pore network, coreflooding, and ultracentrifuge. The porous media consists of two different sets of heterogeneity:

(i) A glass micromodel representing reservoir in the large permeability range (in Darcy).

(ii) A set of sandstone core plugs, representing low-to-medium permeability ranges (in millidarcy).

Six different oil samples of low-to-medium viscosity ranges are used. This paper focuses mainly on the effect of permeability (heterogeneity) on waterflood sweep efficiency.

2. Materials and Equipment

2.1. Brine. 4% ammonium chloride solution in deionized water is used, both as injection and formation waters after filtering through 0.45 micrometer filters. Ammonium chloride brine is used to prevent clay swelling and avoid misleading results, which might occur during waterflooding of Berea sandstone cores.

2.2. Crude Oil. Properties of crude oil can have significant effect on important reservoir properties and hence recovery efficiency. Since properties of crude oil vary to a great extent from one reservoir to another, mainly because of the difference in chemical properties of its heavy polar fractions, we chose to use one crude oil as the base oil and prepared oils of different viscosities by serial dilution with lower molecular weight hydrocarbon solvent. A medium density paraffinic crude oil (896 kg/m^3) with a small acid number (0.04 mg KOH/gm of oil) is collected from a field located in the Arabian Gulf region. After removing associated water and bottom sediments using standard methods, different proportions of light hydrocarbon mixtures (decane and toluene in 80 : 20) are mixed to make five synthetic light viscosity oils. The properties of these samples are in Table 1 including density, viscosity, and interfacial tension with the brine.

2.3. Porous Media. To study the effect of permeability on displacement efficiency, two sets of porous media are used; a layers etched glass pore network and a set of Berea

Table 1: Properties of crude oil samples used for the study.

Sample #	Viscosity* (mPa·s)	Density* (kg/m^3)	Interfacial tension* (mN/m)	Solvent added in 1 liter of crude oil (cm^3)
1	4.3	811	23.39	480
2	6.1	826	23.92	315
3	9.7	833	24.65	200
4	11.2	841	26.06	80
5	23.3	852	26.29	50
6	53.6	866	26.37	0

*The properties were measured at room temperature (298.15 K).

Table 2: Properties of the glass micromodel.

Layer	Depth of etching (10^{-6} m)		Permeability (darcy)	Bulk volume (10^{-6} m^3)	Pore volume (10^{-6} m^3)	Porosity (%)	Pore body diameter (10^{-6} m)
	Pore body	Pore throat					
High k	334	134	42.2	1.02	0.52	51	1059
Medium k	300	120	18.5	0.85	0.28	33	768
Low k	226	90	6.1	0.65	0.15	22	633

sandstone core plugs. The etched glass micromodel is a 2D representation of a small-scale artificial pore network. The etching pattern chosen for this work is spheres with regular shapes. The etched spheres are uniform within a certain layer; however, they differ in size from a layer to another. After the desired network channels are etched on a glass plate using hydrofluoric acid, the inlet and outlet ports are drilled and another glass plate is fused on top of it at 998 K. More details about the fabrication technique of etched glass micromodel can be found elsewhere [11]. The experimental glass micromodel used has three layers of different capillary networks with different pore-throat/pore-body size distributions and absolute permeabilities of 42.2, 18.5, and 6.1 darcy for first, second, and third layers, respectively. These layers are isolated; thereby no cross flow is allowed (Figure 2 and Table 2).

Six Berea sandstone core plugs are used to represent low-to-medium permeability reservoir. These core plugs were subjected to dimension, porosity, permeability, and wettability measurements before waterflood recovery test. These are given in Table 3.

Temco CFS-830-10000-HC reservoir condition coreflooding equipment is used to conduct the coreflooding experiments (Figure 3). The ultracentrifuge used to measure residual saturation is the Corelab ACES 200 model with automated and continuous oil-water interface detection and recovery volume analysis.

Table 3: Petrophysical properties of core plugs.

Core number	Pore volume (10^{-6} m^3)	Porosity (%)	k_{wabs} (10^{-3} D)	Wettability index
1	19.3	20.8	14.1	0.569
2	16.5	20.7	71.3	0.624
3	15.7	19.9	136.2	0.446
4	14.7	20.5	35.0	0.672
5	15.3	21.4	78.0	0.538
6	16.0	20.0	138.3	0.437

Note. All the reported measurements are averages of three trials.

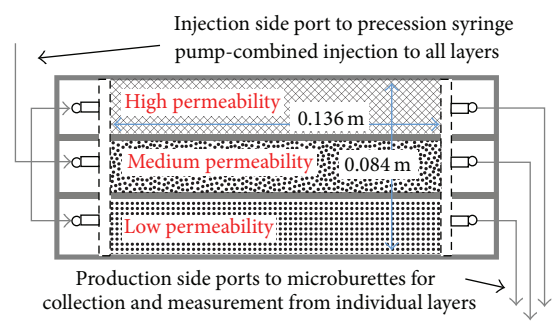

Figure 2: Schematic diagram of the experimental glass micromodel used.

3. Experimental Methods

3.1. Core Preparation. Before waterflood displacement experiments, the cores were cleaned and dried following standard Soxhlet extraction method and a hot air oven. Porosity and permeability measurements were undertaken after satisfactory cleaning and drying, which was followed by brine saturation, oil saturation to S_{oi}, and ageing for 6 weeks in a high pressure aging cell at 50 bar pressure and 373 K temperature.

3.2. Characterization of the Glass Micromodel Pore Network. The glass micromodel used in the study is a chamber-and-throat planar pore network fabricated by photoetching technique. The depth and diameter of pore body-pore throat sizes are measured using a computerized optical stereo microscope capable of measuring depth. In addition, standard falling head method [12] is also used to measure pore characteristics. In both cases the pores were filled with colored water. In the Falling Head Drainage Method, the glass micromodel was

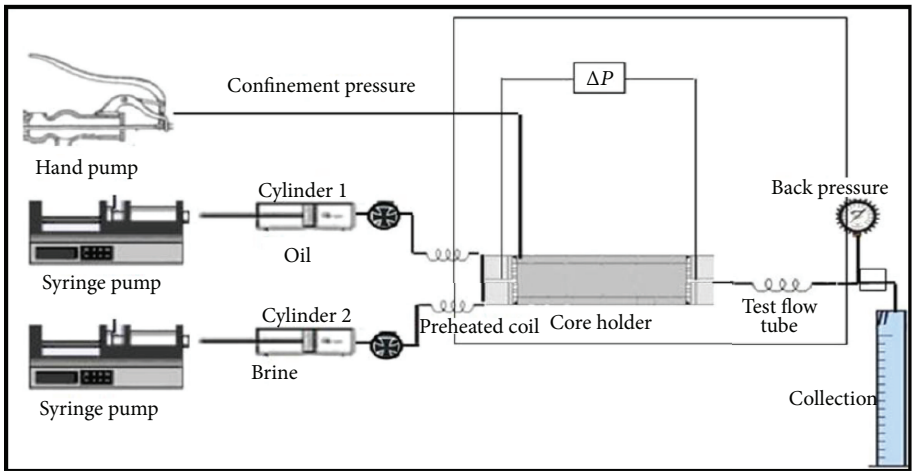

Figure 3: A schematic diagram for coreflooding setup.

100% saturated with colored water, held vertically, and the rate of gravity drainage and the corresponding height of the individual layers were measured at varying hydrostatic head difference. Porosity was measured from the difference of dry and water-filled weight and also using commercially available image analysis software, which provided the total area of the pores and the color contrast between grains and pores. The permeability was measured by falling head method as well as normal horizontal flow using Darcy's equation. Properties of the glass micromodel are in Table 2. The details of experimental procedure applied to measure physical characteristics of the micromodel are given elsewhere [13–16].

3.3. Wettability Measurement. The wettability of the glass micromodel is determined qualitatively through microscopic observation. Once the micromodel is saturated with oil at irreducible water saturation (S_{wirr}), a thin film of water is seen to cover the etched substrate in all the three layers, which indicated the water-wet state of these substrates.

The wettability of the core plugs is determined through conducting spontaneous and forced imbibition and drainage cycles using an ultracentrifuge [17] and Amott Cell. Amott-Harvey wettability indices of the core plugs were determined by the method described by King et al. [18] using the following equation [19]:

$$I_{\text{AH}} = \frac{V_{\text{osp}}}{V_{\text{osp}} + V_{\text{of}}} - \frac{V_{\text{wsp}}}{V_{\text{wsp}} + V_{\text{wf}}}. \quad (2)$$

The wettability index and corresponding rock wettability results are in Table 3.

3.4. Waterflood Recovery. All waterflood experiments were conducted at room temperature and ambient pressure (i.e., there is no back pressure). This was mainly because of the constraints of real-time observation of flow behavior through the attached microscope and camera which was attached with the glass micromodel. Before beginning waterflooding, the glass micromodel pore networks and the core plugs were brought to appropriate saturation profile by flooding with brine followed by crude oil to restore irreducible water saturation (S_{wirr}) condition.

3.5. Waterflood in Glass Micromodel. In the case of glass micromodel, water injection for oil recovery was conducted at volumetric flow rates of 0.167, 0.333, 0.50, 0.833, 1.67, and $2.0 \times 10^{-9}\ \text{m}^3/\text{s}$. At each flow rate, waterflooding was continued until its respective S_{or} state is reached. Water was injected through one single line and flow distribution took place depending on the capillarity and permeability. Flood velocity and capillary numbers on individual layers were calculated from the production rate measured from the opposite side (Figure 2). For the higher viscosity oils, higher flow rates could not be achieved because of the pressure tolerance limit of the pore model. Images were captured at each injection rate and the analysis for oil recovery was performed using the Image Analysis software to calculate recovery percentage [14].

3.6. Waterflood in Core. For the oil recovery measurement in Berea sandstone core plugs, two setups were used: conventional coreflooding and ultracentrifuge method. In conventional coreflooding, the cores (numbers 1, 2, and 3) were loaded in a Hassler type core holder, 3.45×10^3 kPa confinement pressure was applied, and water injection was conducted at incremental flow rates (8.33×10^{-9} to $7.50 \times 10^{-8}\ \text{m}^3/\text{s}$, with an increment of $8.33 \times 10^{-9}\ \text{m}^3/\text{s}$ at each step). The effluent is passed through an oil-water separator equipped with a precession acoustic oil-water interface detection and computation device. Real-time monitoring of oil production and differential pressure across the core were recorded for further use.

3.7. Water Imbibition in Ultracentrifuge. An ultracentrifuge is used to verify and compare the results obtained from coreflooding. In order to have a valid comparison, the rotational speeds were set corresponding to the pressure

difference observed in conventional coreflooding using the following equation [17]:

$$\mathrm{RPM} = \sqrt{\frac{\Delta P}{(0.0000001578) \cdot \Delta\rho \cdot (R_b - L/2) \cdot L}}, \quad (3)$$

where ΔP is the static pressure drop observed in coreflooding experiment, $\Delta\rho$ is the density difference between the displacing and displaced fluids, L is the length of the core used, and R_b is the radius of rotation, which is the distance from the center of the rotor to the end of the core. The oil recovery analysis was performed using a camera which records the shift of oil-water interface. As more oil is produced, the oil-water interface shifts towards the center of the rotor. The associated software considers the stabilized interface position for calculating oil drainage volume. The details of ultracentrifuge measurement process are well documented in public domain [18, 20, 21].

4. Results and Discussion

4.1. Permeability Effect on Displacement Efficiency. Results in this section include the effect of reservoir permeability (heterogeneity) on waterflood displacement efficiency using three sets of experiments, the 2D glass micromodel, the linear flow through coreflooding experiments, and displacement by centrifugal force using ultracentrifuge device, thus, covering both steady state and unsteady state displacements.

4.2. Glass Micromodel. Effect of permeability on displacement efficiency using glass micromodel is shown in Figure 4 for different oil viscosities. In this figure, the waterflood displacement efficiency is plotted against Darcy velocity of water. The setup represented a high permeable noncommunicating stratified reservoir. It is evident that, irrespective of the differences in oil viscosities, the ultimate oil recovery is always higher for the low permeability layer followed by the medium permeability layer and the least recovery is achieved in the high permeability layer. It may also be observed that, for any particular Darcy velocity, the recovery rate follows a similar trend.

During the flow, displacement images were taken at different stages of recovery. Examples of these images can be seen in Figures 5 and 6. The displacement images presented in these figures show the lowest residual oil saturation in the low permeability layer compared to the medium and high permeability layers.

4.3. Coreflooding and Ultracentrifuge. The coreflooding results showing oil displacement efficiency against Darcy velocity for different oil viscosities are shown in Figures 7(a)–7(f). The observations here are similar to that of the etched glass pore network which is lower recovery in high permeability core and vice versa. Oil displacement by forced imbibition (ultracentrifuge) (Figure 8) is in complete agreement with the preceding observations too. At any given pressure drop, the oil recovery is higher for the low permeability core compared to the higher permeability cores.

Therefore, it is evident from all the three waterflood displacement experiments that, at a certain Darcy velocity, higher oil recovery is achievable from lower permeability layers compared to high permeability layers. The above observations are opposed to the conventional knowledge; that is, higher permeability zones lead to higher oil recovery compared to lower permeability zones [22]. The inherent mechanism of such outcomes is further investigated and discussed below.

4.4. Discrepancy at the Microlevel. Water-oil displacement phenomena in porous media are generally viewed and analyzed from a continuum point of view, ignoring the effect of microheterogeneity in the pore level and considering only the average of macroscale properties [23]. Though the Berea core plugs and the etched glass pore network are apparently homogeneous at the macrolevel, it is possible that they possess heterogeneity in the microlevel. This is investigated using X-ray microtomography (Skyscan 1172). From these scans, average pore and grain distribution images are captured and the pore size versus pore number distribution is measured with the help of image analysis software. The pore size distribution in terms of pixel number is presented is Figure 9. It can be seen from this figure that the coefficient of variation in pore size is more for the high and medium permeability cores compared to the low permeability core. Although the core plugs are initially considered as homogeneous, the microtomography images and the pore size distribution show heterogeneity at the microlevel.

The effect of heterogeneity and initial oil saturation on residual oil saturation can be understood using the Initial-residual curve (IRC), which defines the residual saturation of the nonwetting phase at a given initial saturation when the maximum nonwetting saturation attained is available [24].

The IRCs can be characterized using the Land trapping coefficient (C) which is defined as follows [25]:

$$C = \frac{1}{S^*_{\mathrm{nwr}}} - \frac{1}{S^*_{\mathrm{nwi}}}, \quad S^*_{\mathrm{nwi}} = \frac{S_{\mathrm{nwi}}}{1 - S_{\mathrm{wirr}}}, \; S^*_{\mathrm{nwr}} = \frac{S_{\mathrm{nwr}}}{1 - S_{\mathrm{wirr}}}, \quad (4)$$

where S_{wirr} is the irreducible water saturation, S_{nwr} is the residual nonwetting phase saturation, and S_{nwi} is the initial nonwetting phase saturation. The Land trapping coefficient ranges from zero (complete trapping) to infinity (no trapping).

The IRCs and Land trapping coefficient were used to investigate the possible discrepancies in recoveries between the three permeability zones. After calculating "C" values for each flood parameter, the IRC can be constructed by assuming different values for S_{oi} ranging from 0 to 1 and then calculating corresponding S^*_{oi}, followed by calculating corresponding S^*_{or} using "C" value and finally calculating S_{or} value becomes possible. IRCs for the three experimental setups, etched glass pore network, linear coreflooding, and ultracentrifuge, are constructed and presented in Figures 10–12 (due to space limitation, the IRCs of only the lightest oil (4.3 cP) are presented). The analysis performed for each oil sample shows that both microheterogeneity and initial oil saturation affect the attained residual oil saturation, which is consistent for all the three experimental setups.

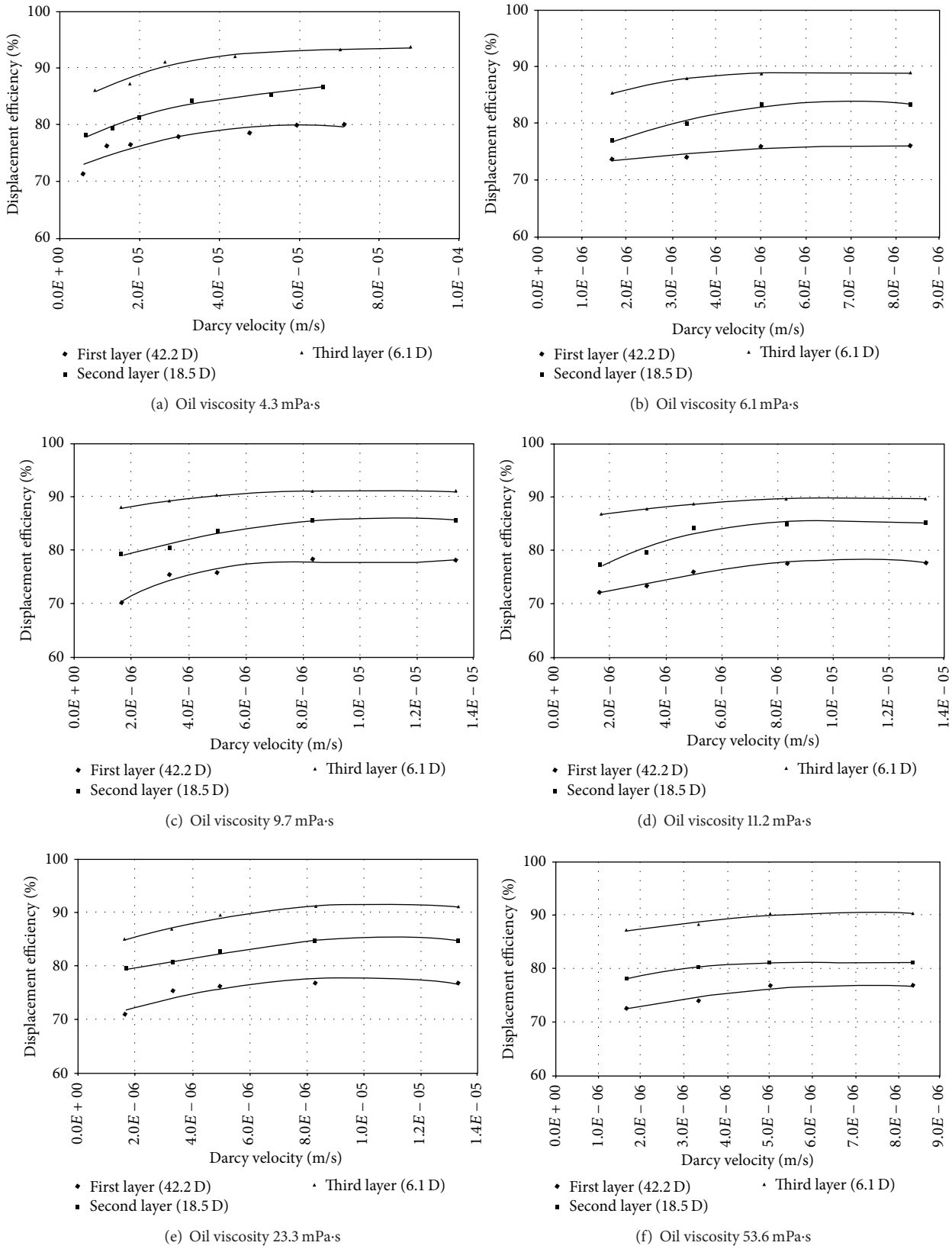

Figure 4: Permeability effect on displacement efficiency (glass micromodel).

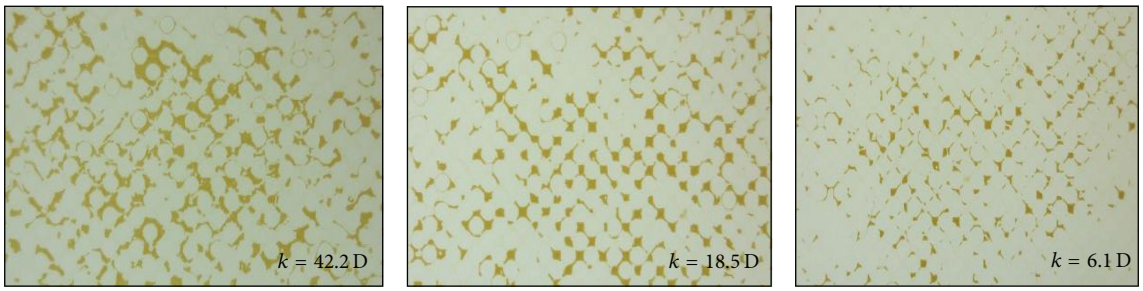

Figure 5: Images of permeability effect on displacement efficiency (oil viscosity 6.1 mPa·s, injection rate 1.70×10^{-9} m^3/s) (glass micromodel).

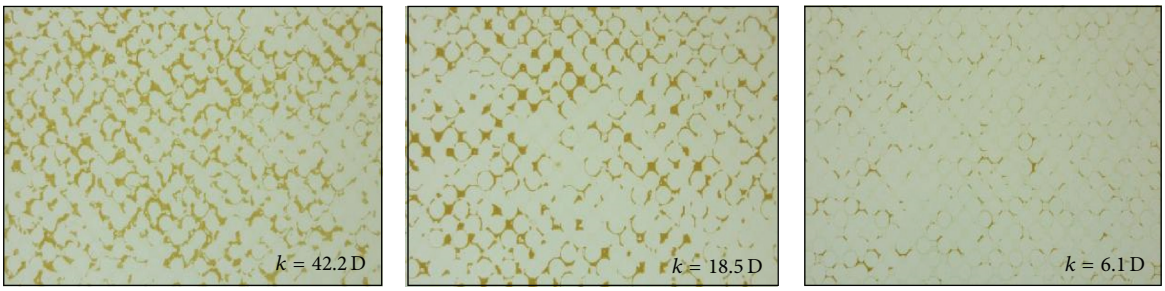

Figure 6: Images of permeability effect on displacement efficiency (oil viscosity 23.3 mPa·s, injection rate 2.72×10^{-9} m^3/s) (glass micromodel).

Figures 10–12 reveal that the effect of microheterogeneity on residual oil saturation is more pronounced than is initial oil saturation, which is consistent in the three experiments conducted. The IRCs show that the high permeability zone (glass micromodel layer and core plug) is more heterogeneous compared to the low permeability zone. Moreover, the calculated Land trapping coefficients are consistent with the previous findings for the three conducted setups (Tables 4–6). The low permeability zone has higher Land trapping coefficient compared to the high permeability zone, which indicates a more homogeneous medium with less oil trapping and hence higher displacement sweep efficiency.

This observation justifies obtaining higher waterflood displacement efficiency from the low permeability zone compared to the high permeability zone. The microheterogeneity created instability in the displacing front, which resulted in low displacement efficiency from the high permeability zone. The microheterogeneity in glass micromodel is represented by the variable pore body, pore throat, and depth of etching within the layer (Table 2). The variability in the dimensions of the pores was created while etching the glass plate using hydrofluoric acid where there is no perfect control on etching the desired channels. Lenormand et al. [26] reported that chemically etched networks on glass plates give clear observations, but the shape of the ducts is not well defined.

In light of the agreement between the results of glass micromodel and both linear coreflooding and ultracentrifuge experiments, there is a high possibility that microheterogeneity presents as well in the Berea sandstone plugs. This microheterogeneity might be the reason for the low displacement efficiency in the high permeability cores. This was supported by conducting X-Ray microtomography on the Berea core plugs used where scans of 2D black and white images were obtained. Three scans for each core were taken, which correspond to injection face, middle of core, and production face. The pore size distribution for each core was determined using image analysis software where the

Table 4: Initial-residual curve (IRC) analysis for glass micromodel (oil viscosity 4.3 mPa·s).

Layer permeability (D)	S_{oi}	S_{or}	S^*_{or}	S^*_{oi}	Land trapping coefficient (C)
42.2	0.821	0.161	0.195	1	4.13
18.5	0.830	0.112	0.133	1	6.55
6.1	0.810	0.050	0.060	1	15.72

Table 5: Initial-residual curve (IRC) analysis for coreflooding (oil viscosity 4.3 mPa·s).

Core permeability (mD)	S_{oi}	S_{or}	S^*_{or}	S^*_{oi}	Land trapping coefficient (C)
136	0.738	0.241	0.318	1	2.14
71	0.772	0.210	0.273	1	2.67
14	0.751	0.181	0.240	1	3.17

Table 6: Initial-residual curve (IRC) analysis for ultracentrifuge (oil viscosity 4.3 mPa·s).

Core permeability (mD)	S_{oi}	S_{or}	S^*_{or}	S^*_{oi}	Land trapping coefficient (C)
138	0.699	0.245	0.351	1	1.85
78	0.659	0.205	0.311	1	2.21
35	0.709	0.163	0.230	1	3.35

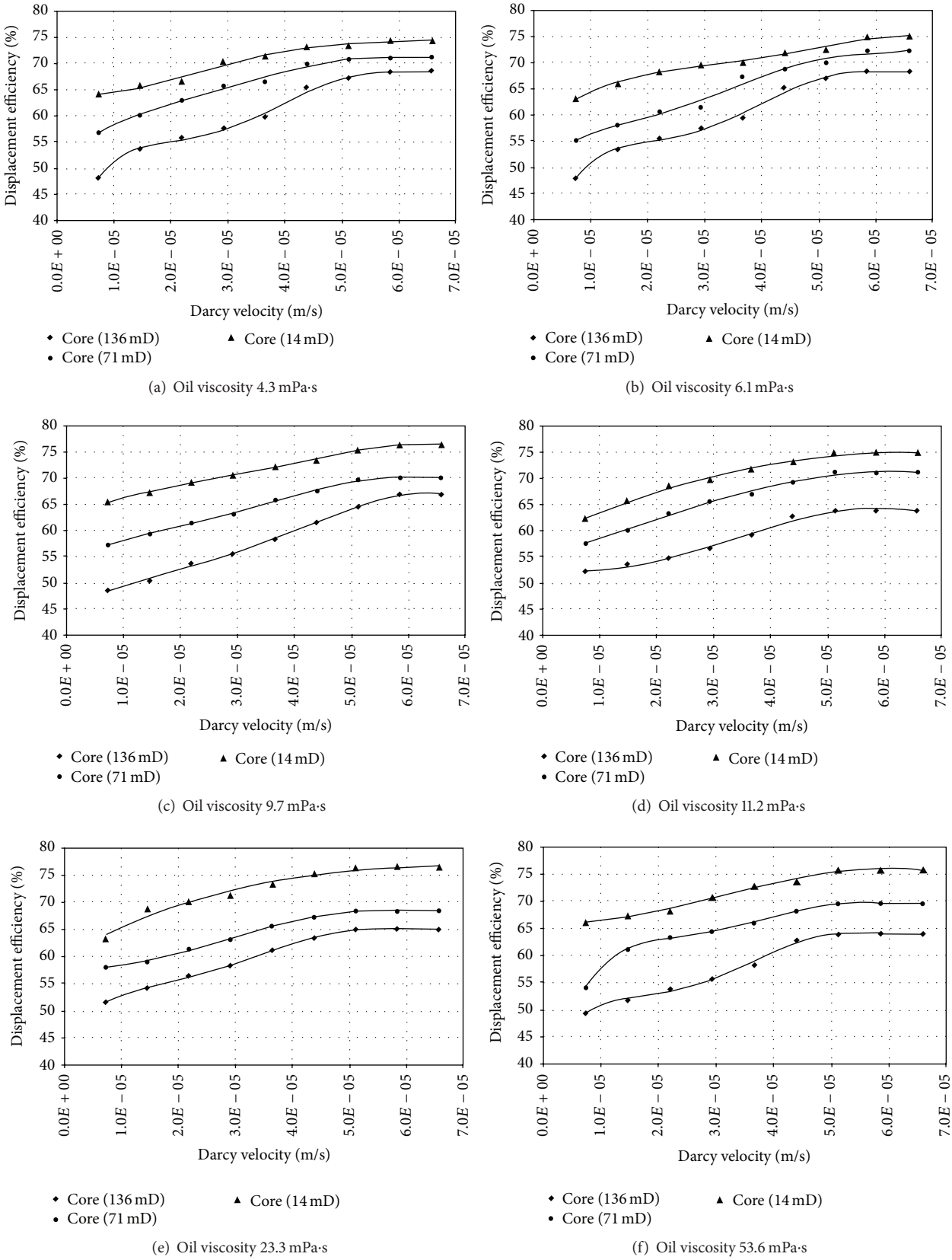

(a) Oil viscosity 4.3 mPa·s

(b) Oil viscosity 6.1 mPa·s

(c) Oil viscosity 9.7 mPa·s

(d) Oil viscosity 11.2 mPa·s

(e) Oil viscosity 23.3 mPa·s

(f) Oil viscosity 53.6 mPa·s

Figure 7: Permeability effect on displacement efficiency as a function of IOIP (coreflooding).

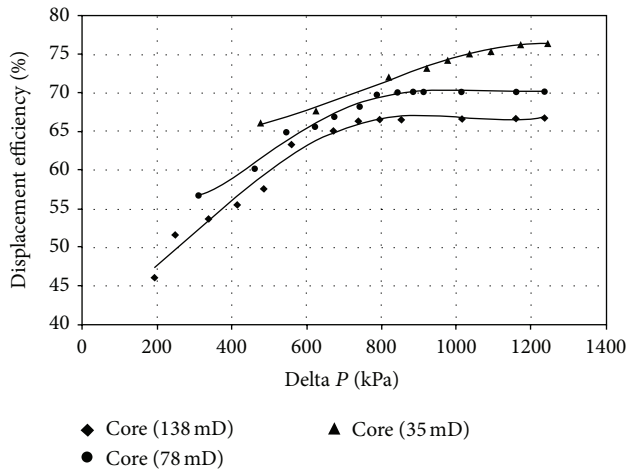

Figure 8: Permeability effect on displacement efficiency (oil viscosity 4.3 mPa·s) (ultracentrifuge device).

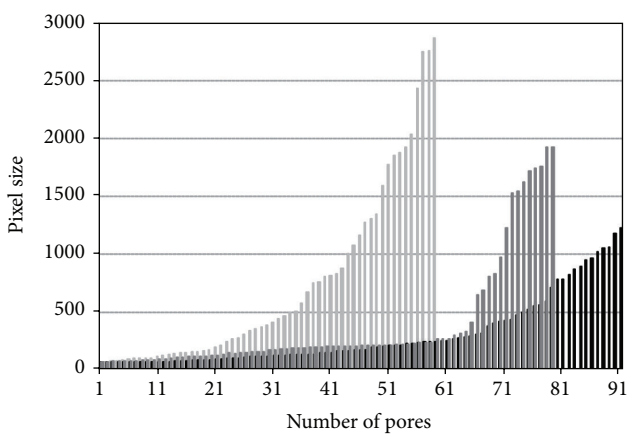

Figure 9: Pore size distribution for cores # 1, 2, and 3 showing higher heterogeneity in higher permeability cores.

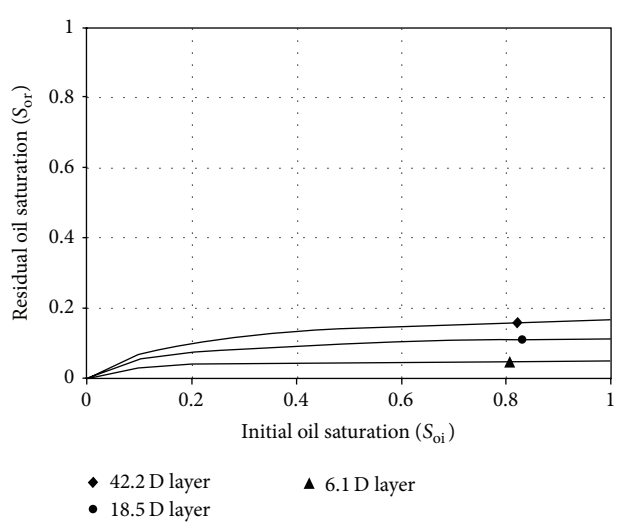

Figure 10: Initial-residual curve (oil viscosity 4.3 mPa·s) (glass micromodel).

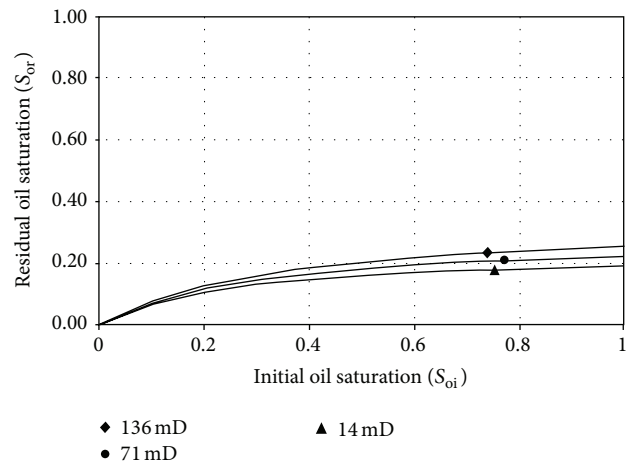

Figure 11: Initial-residual curve (oil viscosity 4.3 mPa·s) (coreflooding).

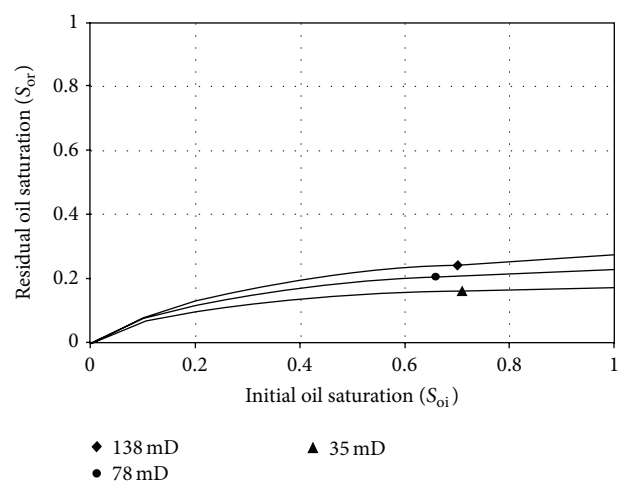

Figure 12: Initial-residual curve (oil viscosity 4.3 mPa·s) (ultracentrifuge device).

distribution is expressed in terms of pixel numbers. Figure 9 shows an example of pore size distribution for the cores used in coreflooding (cores numbers 1, 2, and 3). Figure 9 confirms that the microheterogeneity level is the highest for the high permeability core and the lowest for the low permeability core, which could be the reason for the lower waterflood efficiency in high permeability core compared to that of low permeability. These observations are in agreement with Francisca and Montoro [27]. They reported more uniform displacement of the nonwetting phase in low permeable fine sand compared to the higher permeability medium and coarse sands. Microscale heterogeneities and formation of ganglia are attributed to these phenomena, even though the systems used were homogeneous at macroscale, similar to the present work.

4.5. Discrepancy at the Macrolevel. The advantage of etched glass pore network displacement studies is the visual observation of the fingering phenomenon which arose during

Figure 13: Fingering in glass micromodel at the lowest applied rate of 0.167 mm^3/s.

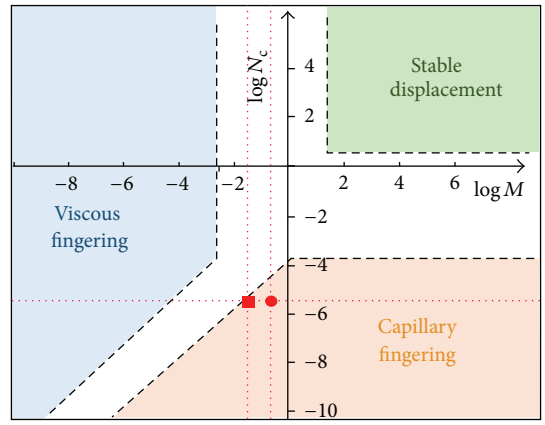

Figure 14: Phase diagram for different displacement forms (modified from [30]).

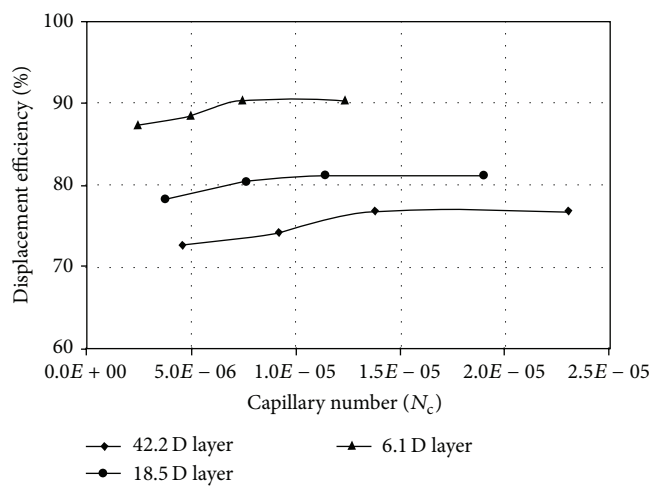

Figure 15: Waterflood displacement efficiency versus capillary number (oil viscosity 53.6 mPa·s) (glass micromodel).

the displacement. Out of numerous images captured, a representative one is presented in Figure 13. A line is drawn on the water front for clear visibility of the fingering pattern. It is evident that the fingers at the high permeability layer were left behind large areas of unswept oil compared to the other two layers. Moreover, the figure shows that the lowest number of fingers was developed in the low permeability layer, which justifies higher recovery compared to other layers.

During immiscible displacement, the forces exist at the interface and influencing the frontal instability includes gravity, viscosity, and interfacial tension [28]. For immiscible displacements upon which only viscous and capillary forces are acting (being horizontal flow, gravity can be ignored), the expected displacement patterns are either stable front displacement or unstable front displacement. In the latter case the instability arises due to either capillary or viscous fingering depending on capillary number (N_c) and viscosity ratio (M).

Lenormand [29] constructed a phase diagram to characterize different regimes of instability based on a wide range of mobility ratios and capillary numbers, which can be used as a qualitative guideline to explain the observed phenomena in the present work. Lenormand et al. [30] further reported the conditions for shifting from one displacement form to another based on experimental and simulation works. If the viscosity ratio (injected fluid/displaced fluid) M is significantly less than 1, it is expected to find capillary fingering at relatively low flow rate and viscous fingering at relatively high flow rate. On the other hand, when the viscosity ratio is greater than one, the two basic forms of immiscible displacement are capillary fingering at relatively low flow rate and stable displacement at relatively high flow rate.

For the experimental works conducted in this paper, the first condition applies as the viscosity of injected water is less than the viscosity of displaced oil. Hence, the displacement form could be either capillary fingering at relatively low injection rates or viscous fingering at higher injection rates. Each pore network in the micromodel has its own phase diagram, so as a qualitative measure we decided to use the phase diagram proposed by Lenormand et al. [30] (Figure 14).

In our case, the capillary number applied is about 10^{-6}–10^{-5}, and the viscosity ratios are 0.2 and 0.02 for the lightest and heaviest oils, respectively. Figures 15 and 16 show the capillary pressure applied in glass micromodel and coreflooding experiments, respectively. From Figure 14, we can see that capillary fingering is the dominating cause of frontal instability based on the capillary number applied and viscosity ratios used. For illustration, a circle is placed on the phase diagram for the condition of the lightest oil and a square for the heaviest oil used.

Capillary fingering is characterized by fingers that spread across the whole network and grow in all directions and can be best described using the invasion percolation (IP) theory. However, very thin and more dendritic fingers form in the viscous fingering domain, which can be characterized using the diffusion-limited aggregation (DLA) theory. Figure 13 supports the domination of capillary fingering as the fingers grow in all directions and do not look very thin as in the case of viscous fingering domain.

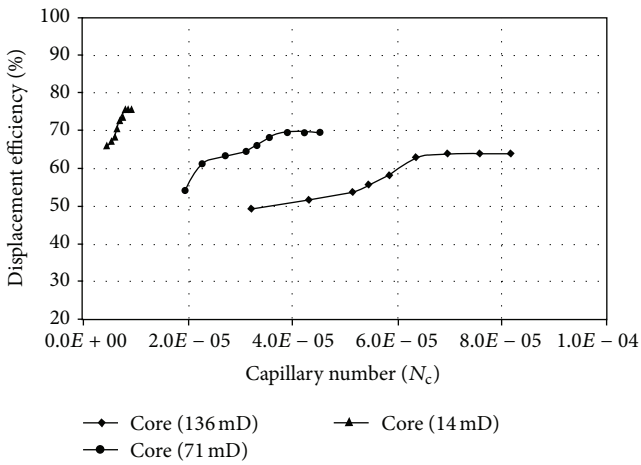

Figure 16: Waterflood displacement efficiency versus capillary number (oil viscosity 53.6 mPa·s) (coreflooding).

Lenormand et al. [30] also reported that capillary fingering results in higher oil recovery compared to viscous fingering and there is a transition zone in between. Hence, oil recovery decreases with increasing capillary number as the instability changes from capillary to viscous fingering at a certain viscosity ratio. It must be noted that this phase diagram is drawn based on computer simulation in which oil displaced water and wettability are not taken into consideration. Thus, it is a case of drainage, whereas in our case it is a pure case of imbibition, as water displaced oil in water-wet media. The phase diagram thus should be considered as indicative only. This is explained in the work of Trojer et al. [31], in which the work of Lenormand is extended to different wettability situations.

Based on our findings, there is a high possibility that the low permeability layer lies more into the capillary fingering domain; however, the high permeability layer, which has a higher capillary number, moves towards the viscous fingering domain, which justifies the lower displacement efficiency in higher permeability layers. Figure 15, which depicts an example of capillary number and displacement efficiency relationship for the three layers of the glass micromodel, shows that the low permeability layer has the lowest applied capillary number, which corresponds to the highest oil recovery among other layers in a capillary dominated region. It is worth mentioning that each 3 points (point in each layer) in Figure 15 correspond to a certain total flow rate; however, as the flow is commingled then each layer has its own share of that flow rate based on its permeability, which is translated into different capillary numbers. Nevertheless, in the same figure we can see the increase in displacement efficiency from individual layers with increasing the capillary number; hence there is a possibility that the displacement form is shifting to the viscous fingering region at higher rates. The previous observations holds true for coreflooding experiments too (Figure 16).

4.6. Conformance Issue. In a commingled water injection system, water is injected into all the zones through a single injection well (Figure 1(b)). This results in disproportionate flow of water. The highest permeability layer receives the most water followed by the medium and least water flows through the low permeability layers. It is often the case that the low permeable layers do not receive enough water necessary to achieve the minimum Darcy velocity required for optimum sweep efficiency. For example, it may be seen from Figure 7(a) that, to achieve 65% oil recovery, the required Darcy velocity is (1.46, 2.92, and 4.38) $\times 10^{-5}$ m/s in the low, medium, and high permeability layers, respectively. Nevertheless, considering the permeability ratio of approximately 1 : 5 : 10 (the present case) and the fact that the water flow follows Darcy's law, this proportionality of flow rate or Darcy velocity is not achievable for the low permeability layer. If water injection rate is increased to achieve the minimum flow requirement in the low permeability layers, there will be a huge amount of breakthrough water production through the high permeability layers and the entire project will become uneconomical.

Also, it is possible that, after the water breakthrough due to the increase in water saturation, the relative permeability of high permeability layer will increase progressively until the endpoint relative permeability. Consequently, the relative proportion of water flow through the low permeability layer would reduce further resulting in further deprivation of flood water in the low permeability layer. This effect of disproportionate flow is more pronounced when fingering phenomena are present.

The findings of this paper supported by both experimental data and visual observations explain why a commingled waterflood would result in a poor oil recovery from low permeability stratum though its ultimate recovery potential is higher. Nevertheless, in both cases, recovery can be improved by regulating water flow in proportion to optimum Darcy velocity in each layer and hence maximize recovery potential.

4.7. Possible Uncertainties in Experimental Results. In the area of petroleum/reservoir engineering research, there are two major sources of uncertainty: (1) systematic errors originated from the experimental model because it is impossible to create a true representation of actual oil reservoirs [32] and (2) random error or measurement errors in the experiments performed to determine a parameter. The factors which may contribute to systematic errors in oil recovery analysis are as follows: (1) porosity, permeability, tortuosity, wettability, clay and other mineral contents, surface charge, and microheterogeneity of the porous medium, (2) composition, polarity, and suspended materials in the oil, and (3) composition and suspended particles in the brine. The precautions taken in this work to minimize systematic errors are mimicking an oil reservoir through using two sets of porous media (a glass micromodel and a set of Berea sandstone core plugs), which are considered to be near ideal in the petroleum engineering research. A single oil sample was used in the experiments and it was diluted to meet viscosity requirements.

Major random errors in determining oil recovery may arise from porosity, core saturation, and recovery volume measurements. The minor errors may result from oil viscosity, fluid compressibility, expansion or compression of rock pore volume during displacement, and changes in

rock wettability due to migration of pore lining clay during flooding. Couple of precautions were taken to minimize the random errors including the following: (1) porosity measurements were conducted using Helium gas, which obeys ideal gas law and all pressure gauges were calibrated before use; (2) saturation of core plugs was conducted under constant and regulated room temperature to avoid thermal expansion/compression of rock and fluids; (3) repeated weight measurements were conducted during core saturation process to ensure maximum fluid saturation; (4) oil recovery measurements were conducted with the help of an online calibrated acoustic interface measurement. This online measurement eliminates the possibilities of oil evaporation loss; (5) for most of the measurements conducted, an average value of three trials was taken.

In spite of all the above measures, systematic and random errors cannot be eliminated. McPhee and Arthur [33] observed up to 20% variation of data despite using similar test core plugs, identical test fluids, and similar test procedures in core saturation and recovery measurements from interlaboratory results. The results are within an acceptable limit of 5% when the experiments are performed in one laboratory. In the present study, maximum efforts were given to minimize random error in determining rock wettability, oil viscosity, and flow pressure measurement following standard guidelines [34] and 95% confidence interval is expected.

Nevertheless, uncertainty in reservoir engineering calculation cannot be eliminated unless the data are in the range of millions and sophisticated software is used to analyze them. The results presented in these articles are used mainly for comparison purpose and should be considered as indicative and not for quantitative estimation. For quantitative estimation of recovery, a target reservoir has to be identified, and well preserved actual reservoir core and live reservoir oil sample have to be used.

5. Summary and Conclusions

Waterflood recovery efficiency investigated through two sets of porous media with large permeability contrast, representing commingled waterflood in a stratified reservoir with vertical permeability discontinuity, is described. The major findings of this study are as follows:

(i) Glass micromodel within the permeability range of a few Darcy was used to represent high permeable reservoirs and Berea sandstone core plugs were used to represent low-to-medium permeable reservoirs. In all cases, the ultimate recovery potential was higher for the low permeability layer followed by the medium permeability layer and least recovery was achieved in the high permeability layer.

(ii) This observation is consistent irrespective of huge difference of viscosity, flood water velocity, permeability range, and measurement method.

(iii) At microscopic level, microheterogeneity and capillary fingering phenomena could be the reason behind this observation. The fingering effect was supported by displacement images through glass micromodel.

(iv) In a commingled waterflood project, low permeability layers will be poorly swept by waterflood because of deprivation of required volume of water compared to high permeability layers. This study highlighted an exceptional case when fingering occurs in the higher permeability zone. Downhole flow controller or injection water profile modification is recommended in such cases before beginning water injection.

Nomenclature

C: Land trapping coefficient, dimensionless
E_A: Areal sweep efficiency, percentage
E_D: Displacement sweep efficiency, percentage
E_I: Vertical sweep efficiency, percentage
E_V: Volumetric sweep efficiency, percentage
I_{AH}: Amott-Harvey wettability index, dimensionless
k: Permeability of porous media, D
k_{wabs}: Absolute water permeability, D
L: Core length, m
M: Viscosity ratio, fraction
N_c: Capillary number, dimensionless
R_b: Radius of rotation, m
RE: Recovery efficiency, percentage
RPM: Revolutions per minute
S_{nwi}: Initial saturation of nonwetting phase, fraction
S_{nwr}: Residual saturation of nonwetting phase, fraction
S_{oi}: Initial oil saturation, fraction
S^*_{oi}: Normalized initial oil saturation, fraction
S_{or}: Residual oil saturation, fraction
S^*_{or}: Normalized residual oil saturation, fraction
S_{wirr}: Irreducible water saturation, fraction
V_{of}: Volume of oil produced by forced water imbibition, cm^3
V_{wf}: Volume of water produced by forced oil drainage, cm^3
V_{osp}: Volume of oil produced by spontaneous water imbibition, cm^3
V_{wsp}: Volume of water produced by spontaneous oil drainage, cm^3
ΔP: Pressure drop, psi
$\Delta\rho$: Density difference between displacing and displaced fluids, kg/m^3
σ: Interfacial tension, dynes/cm.

Competing Interests

The authors declare that they have no competing interests.

Acknowledgments

The authors are grateful to the Petroleum Engineering Department, The Petroleum Institute, Abu Dhabi, for providing the laboratory facilities to conduct the laboratory experiment.

References

[1] L. W. Lake, *Enhanced Oil Recovery*, Prentice Hall, Engelwood Cliffs, NJ, USA, 1989.

[2] N. El-Khatib, "Waterflooding performance of communicating stratified reservoirs with log-normal permeability distribution," *SPE Reservoir Evaluation and Engineering*, vol. 2, no. 6, pp. 542–549, 1999.

[3] G. P. Willhite, *Waterflooding*, vol. 3 of *SPE Textbook Series*, Society of Petroleum Engineers, Richardson, Tex, USA, 1986.

[4] A. Mai and A. Kantzas, "Heavy oil waterflooding: effects of flow rate and oil viscosity," *Journal of Canadian Petroleum Technology*, vol. 48, no. 3, pp. 42–51, 2009.

[5] K. Langaas and S. Nilsson, "Pore-scale simulations of disproportionate permeability reducing gels," *Journal of Petroleum Science and Engineering*, vol. 25, no. 3-4, pp. 167–186, 2000.

[6] S. Nilsson, A. Stavland, and H. C. Jonsbraten, "Mechanistic study of disproportionate permeability reduction," in *Proceedings of the SPE/DOE Improved Oil Recovery Symposium*, SPE-39635-MS, Tulsa, Okla, USA, April 1998.

[7] S. M. El-Hadidi, G. K. Falade, C. Dabbouk, and F. Al-Ansari, "Water injection profile modification in a layered reservoir with polymer treatment," *SPE Reservoir Evaluation and Engineering*, vol. 3, no. 3, pp. 197–203, 2000.

[8] R. S. Seright, J.-T. Liang, W. B. Lindquist, and J. H. Dunsmuir, "Characterizing disproportionate permeability reduction using synchrotron X-ray computed microtomography," *SPE Reservoir Evaluation & Engineering*, vol. 5, no. 5, pp. 355–364, 2002.

[9] L. A. Amy, S. A. Peachey, A. R. Gardiner, G. E. Pickup, E. J. Mackay, and K. D. Stephen, "Recovery efficiency from a turbidite sheet system: numerical simulation of waterflooding using outcrop-based geological models," *Petroleum Geoscience*, vol. 19, no. 2, pp. 123–138, 2013.

[10] B. Rashid, A. H. Muggeridge, A. Bal, and G. Williams, "Quantifying the impact of permeability heterogeneity on secondary-recovery performance," *SPE Journal*, vol. 17, no. 2, pp. 455–468, 2012.

[11] I. Chatzis, N. R. Morrow, and H. T. Lim, "Magnitude and detailed structure of residual oil saturation," *Society of Petroleum Engineers journal*, vol. 23, no. 2, pp. 311–326, 1983.

[12] C. Liu and J. Evett, *Soils and Foundations*, Prentice Hall, Upper Saddle River, NJ, USA, 2001.

[13] S. F. Shariatpanahi, A. Dastyari, B. Bashukooh, M. Haghighi, M. Sahimi, and S. S. Ayatollahi, "Visualization experiments on immiscible gas and water injection by using 2D-fractured glass micromodels," in *Proceedings of the SPE Middle East Oil and Gas Show and Conference*, vol. 93537, pp. 907–915, Manama, Bahrain, March 2005.

[14] A. S. Ibrahim, "Investigation of the mobilization of residual oil using micromodels," in *Proceedings of the SPE Annual Technical Conference and Exhibition*, Paper SPE 129515, New Orleans, La, USA, 2009.

[15] M. H. Ghazanfari, R. Kharrat, D. Rashtchian, and S. Vossoughi, "Statistical model for dispersion in a 2D glass micromodel," *SPE Journal*, vol. 15, no. 2, pp. 301–312, 2010.

[16] E. W. Al-Shalabi, *Understanding waterflood recovery efficiency through porous media and enhancing recovery using DC potential [M.S. thesis]*, The Petroleum Institute, Abu Dhabi, UAE, 2010.

[17] *Corelab ACES 200 Rock-Core Ultracentrifuge*, User Manual, Tulsa, Okla, USA, 2010.

[18] M. J. King, K. R. Narayanan, and A. J. Falzone, "Advances in centrifuge methodology for core analysis," in *Proceedings of the SCA International Symposium on Core Analysis*, Paper No. SCA-901, Dallas, Tex, USA, 1990.

[19] N. Hadia, H. H. Lehne, K. G. Kumar, K. Selboe, J. A. Stensen, and O. Torsaeter, "Laboratory investigation of low salinity waterflood on reservoir rock samples from the froy field," in *Proceedings of the SPE Middle East Oil and Gas Show and Conference*, SPE-141114-MS, Manama, Bahrain, September 2011.

[20] G. Glotin, J. Genet, and P. Klein, "Computation of drainage and imbibition capillary pressure curves from centrifuge experiments," in *Annual Technical Conference and Exhibition*, vol. 20502 of *Proceedings of SPIE*, pp. 313–324, New Orleans, La, USA, September 1990.

[21] M. Fleury, P. Poulain, and G. Ringot, "A capacitance technique for measuring production while centrifuging," in *Proceedings of the International Symposium of the Society of Core Analysts*, Paper No. SCA-9833, The Hague, The Netherlands, September 1998.

[22] N. C. Wardlaw, "The effects of pore structure on displacement efficiency in reservoir rocks and in glass micromodels," in *Proceedings of the SPE/DOE Enhanced Oil Recovery Symposium*, SPE-8843-MS, Tulsa, Okla, USA, April 1980.

[23] A. G. Yiotis, A. K. Stubos, A. G. Boudouvis, and Y. C. Yortsos, "A 2-D pore-network model of the drying of single-component liquids in porous media," *Advances in Water Resources*, vol. 24, no. 3-4, pp. 439–460, 2001.

[24] G. L. Stegemeier, "Mechanisms of entrapment and mobilization of oil in porous media," in *Improved oil Recovery by Surfactant and Polymer Flooding*, pp. 55–91, Academic Press, New York, NY, USA, 1977.

[25] C. S. Land, "Calculation of imbibition relative permeability for two- and three-phase flow from rock properties," *SPE Journal*, vol. 8, no. 2, pp. 149–156, 1968.

[26] R. Lenormand, C. Zarcone, and A. Sarr, "Mechanisms of the displacement of one fluid by another in a network of capillary ducts," *Journal of Fluid Mechanics*, vol. 135, pp. 337–353, 1983.

[27] F. M. Francisca and M. A. Montoro, "Micro-scale analysis of immiscible displacement in porous media," in *Proceedings of the 13th Pan-American Conference on Soil Mechanics and Geotechnical Engineering*, Margarita Island, Venezuela, July 2007.

[28] G. M. Homsy, "Viscous fingering in porous media," *Annual Review of Fluid Mechanics*, vol. 19, pp. 271–311, 1987.

[29] R. Lenormand, "Capillary and viscous fingering in an etched network," in *Physics of Finely Divided Matter*, vol. 5 of *Springer Proceedings in Physics*, pp. 289–294, Springer, Berlin, Germany, 1985.

[30] R. Lenormand, E. Touboul, and C. Zarcone, "Numerical models and experiments on immiscible displacements in porous media," *Journal of Fluid Mechanics*, vol. 189, pp. 165–187, 1988.

[31] M. Trojer, M. L. Szulczewski, and R. Juanes, "Stabilizing fluid-fluid displacements in porous media through wettability alteration," *Physical Review Applied*, vol. 3, no. 5, 2015.

[32] T. Bu and E. Damsleth, "Errors and uncertainties in reservoir performance predictions," *SPE Formation Evaluation*, vol. 11, no. 3, pp. 194–200, 1996.

[33] C. A. McPhee and K. G. Arthur, "Relative permeability measurements: an inter-laboratory comparison," in *Proceedings of the SPE European Petroleum Conference*, Paper SPE 28826, pp. 199–211, London, UK, October 1994.

[34] F. M. Pellerin and B. Zinszner, *A Geoscientist's Guide to Petrophysics*, IFP Publications, Technip, Paris, France, 2007.